FINE STRUCTURE OF THE PROTON–PROTON AND ANTIPROTON–PROTON DIFFRACTION CONE AT LHC ENERGIES

N. Bence[1] , I. Szanyi[2,3,4] , A. Lengyel[5]

[1] Uzhhorod National University, 14, Universytets'ka St., Uzhhorod,
[2] Wigner RCP, POB 49, Budapest, 1525, Hungary,
[3] Eötvös University, Pázmány P. s. 1/A, Budapest, 1117, Hungary,
[4] MATE Institute of Technology, Károly Róbert Campus, H-3200 Gyöngyös, 36, Mátrai St., Hungary,
[5] Institute of Electron Physics of NAS of Ukraine, 21, Universytets'ka St., Uzhhorod,
e-mails: bencenorbert007@gmail.com, istvan.szanyi@cern.ch, alexanderlengyel39@gmail.com

The local nuclear curvature $C(s,t)$ as a derivative of local nuclear slope $B(s,t)$ is reconstructed from the experimental differential cross-section of pp and $\bar{p}p$ elastic scattering for TeV energies in the small-$|t|$ region where the non-exponential behavior of the diffraction cone, i.e. the "break" phenomenon is clearly visible. Predictions for $C(s,t)$ are investigated in several Pomeron models. The extreme sensitivity of the local nuclear curvature for the choice of a Pomeron model is emphasized. Only some of them predict a $C(s,t=0)$ or $\langle C(s) \rangle$ which decreases with energy and changes sign at very large energy.

Key words: Pomeron, Odderon, asymptopia, pp and $\bar{p}p$ elastic scattering, local nuclear curvature, local nuclear slope.

I. INTRODUCTION

The TOTEM experiment at CERN LHC observed the non-exponential behavior of the low-$|t|$ elastic pp differential cross-section, i.e. the so called "break" phenomenon at $\sqrt{s} = 8$ and 13 TeV colliding energies in a statistically significant manner [1–3]. The analysis revealed that the differential elastic cross section does not, in fact, decrease purely exponentially as $\exp(-B|t|)$ at a small value of $|t|$, but rather shows a concave curvature relative to the expected exponential decrease as in the case of pp elastic scattering measurements at ISR in the 1970s. Recently, it was found that the curvature effects, although small, lead to significant changes in the forward slope parameter relative to that determined in a purely exponential fit. This suggests the inclusion of the small-$|t|$ differential cross section data into the fits [4]. Curvature was studied previously at much lower energies in Refs. [5, 6].

Below we propose a simple procedure to reveal the "experimental" curvature allowing us to assess the onset of the asymptopia. The onset of asymptopia coincides with the energy where the value of the curvature parameter at vanishing $|t|$ goes to zero. Therefore, we shall study the energy and $|t|$ behaviour of the curvature within the framework of phenomenological models. These models naturally consider the curvature as a manifestation of the threshold structure of the scattering amplitude required by t-channel unitarity.

II. CHOICE OF DATA AND CURVATURE SHAPE

Latest experiments on elastic pp scattering performed at CERN brought us closer to answering an old question: "where is asymptopia?" [7]. In elastic hadron–hadron scattering the fine structure parameters of diffraction cone such as the slope

$$B(s,t) = \frac{d}{dt} \ln \left(\frac{d\sigma(s,t)}{dt} \right), \qquad (1)$$

and curvature

$$C(s,t) = \frac{1}{2} \frac{d}{dt} B(s,t), \qquad (2)$$

are sensitive indicators of the transition to the "asymptotic" regime [8]. To further explore the above mentioned non-exponential behavior, we shall use the experimental data points at a given fixed energy normalized by a linear exponential [1, 2]:

$$R_{\exp}(t) = \frac{\left(\frac{d\sigma}{dt} \right)_{\exp} - \left(\frac{d\sigma}{dt} \right)_{\lin}}{\left(\frac{d\sigma}{dt} \right)_{\lin}}, \qquad (3)$$

where $(d\sigma/dt)_{\exp}$ are the measured data points and $(d\sigma/dt)_{\lin}$ is the approximation of all experimental points at given fixed energy in a selected interval of $|t|$ by a linear exponential i. e.

$$\left(\frac{d\sigma}{dt} \right)_{\lin} = ae^{bt}, \qquad (4)$$

with a and b fitted to the data. The result of applying this procedure is illustrated in Fig. 1.

Below we propose a simple procedure to obtain the "experimental" curvature enabling us to assess the offensive of the mentioned asymptotic regime. For this purpose, we select a range of interest in the diffraction cone, i. e. a $|t|$ range showing the "break" phenomenon, which is likely a reflection due to the "pion cloud" [9]. On one hand, the boundary of this range is determined by

the Coulomb-nuclear interference region of the diffraction cone $|t_c|$. In general, the above boundary reaches the value $|t| \approx 0.01$ GeV^2 but not less than $|t| = 0.005$ GeV^2. The other boundary for large-$|t|$, $|t_d|$, does not reach the dip-bump region, which is for a few tens of GeV energies at $|t| \approx 1$ GeV^2, and for TeV energies at $|t| \approx 0.6 - 0.2$ GeV^2. Within these boundaries, one can find the area where the $R(t)$ normalized differential cross-sections have concave shapes (see, for example, Fig. 1) reflecting the presence of the "break" observed first at ISR in the 1970s [10]. This phenomenon was detected with a greater or lesser precision in subsequent experiments: SPS, Tevatron and LHC. The precision is associated with the specifics of the experiment.
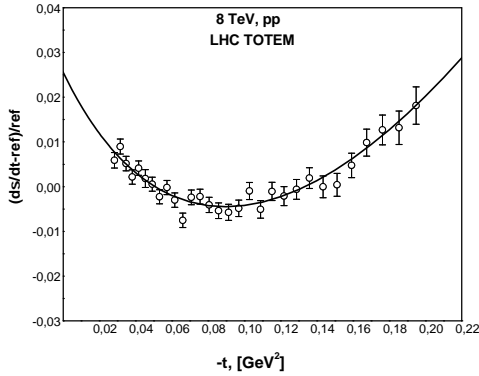
1a
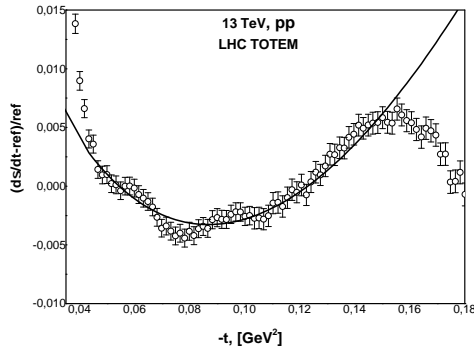
1b

Fig. 1. The normalized differential cross section for pp scattering at 8 TeV (1a) [1] and 13 TeV (1b) [2]. Open circles together with the bars are the experimental points with statistical errors. The black curves are a theoretical R-function calculated from the model defined by Eq. (5) fitted to the experimental points

In this work, we study the s- and t-behavior of the curvature within the framework of the phenomenological approach which considers the "break" as the revelation of the threshold structure of the scattering amplitude in the t-channel and the shape of proton in the kinematic region in question. Doing this, we choose the following non-exponentially behaving model for the differential cross section within the diffraction cone at a fixed energy [9, 11]:

$$\frac{d\sigma(t)}{dt} = ae^{\delta t + \gamma \sqrt{t_0 - t}}, \qquad (5)$$

where $t_0 = 4m_\pi^2$.

In addition, to find the interval of the momentum transfer for the experimental data, where it is necessary to carry out the investigations, we used the same normalized form $R_{\text{th}}(t)$, as defined above:

$$R_{\text{th}}(t) = \frac{\left(\dfrac{d\sigma}{dt}\right)_{\text{th}} - \left(\dfrac{d\sigma}{dt}\right)_{\text{lin}}}{\left(\dfrac{d\sigma}{dt}\right)_{\text{lin}}}, \qquad (6)$$

where $(d\sigma/dt)_{\text{th}}$ is the theoretical differential cross section, Eq. (5) fitted to the experimental points and $(d\sigma/dt)_{\text{lin}}$ is the approximation of all experimental points with the model given by Eq. (4) at a given fixed energy. Within the model given by Eq. (5), the slope and curvature can be calculated with the help of Eqs. (1) and (2). To look for the fine structure of the diffraction cone of pp and $\bar{p}p$ elastic scattering at LHC energies and close to it, we chose the experimental data for pp and $\bar{p}p$ elastic scattering which contain a sufficiently large number of experimental points N, and the concave form of the function R is clearly visible. Namely, we consider the energies: E_{cm}=546 GeV for $\bar{p}p$ scattering [12, 13] and 7 TeV (ATLAS) [14], 8 TeV [1], 13 TeV [2, 3] for pp scattering. Another aspect is that the χ^2/NDF value in the investigated range in the case of the fits with model (5) should be as close to 1 as possible (the eighth column in Table 1 with statistical error accounting only). As a result, we find the so-called *"experimental"* values of the curvature within the selected kinematical region for all the selected 5 sets by model (5). The results are shown in Fig. 2 and quoted in Table 1. Note that in the case of the measurements at 1.8 [15] and 1.96 TeV [16] for $\bar{p}p$ scattering, and also at 2.76 TeV [17] and 7 TeV (TOTEM) [18], the slope $B(s,t)$ is almost constant ($C(s,t) = 0$); thus these data were not included in our analysis.

Set	$\sqrt{s}$, GeV^2	$|t_c|$, GeV^2	$|t_d|$, GeV^2	$C(0)$, GeV^{-4}	$\Delta C(0)$, GeV^{-4}	N	χ^2/NDF	Exp. data
1	546	0.0157	0.6200	10.53	0.94	135	1.26	[12, 13]
2	7000	0.0132	0.1668	8.80	1.66	25	0.61	[14]
3	8000	0.0285	0.1947	8.34	0.65	30	0.95	[1]
4	13000 (1)	0.0305	0.1662	7.20	1.29	76	0.90	[2]
5	13000 (2)	0.0466	0.1589	7.98	0.35	67	0.95	[3]

Table 1. The boundaries of diffraction cone regions and relevant curvature values for selected energies
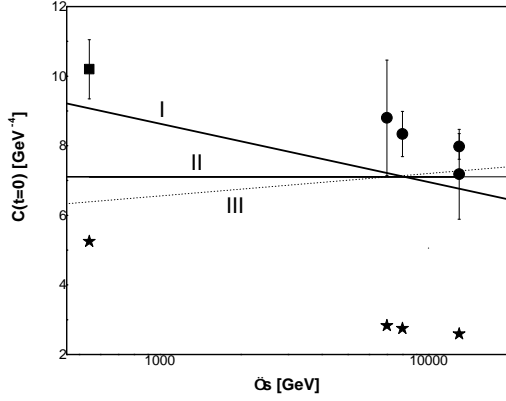
Fig. 2. The *"experimental"* curvature $C(s,0)$ calculated by Eqs. (1), (2), (5) with the parameters obtained from the fit using model (5) for all 5 selected sets of experimental data. The black circles represent pp scattering, the black square represents $\bar{p}p$ scattering. The bar represents the fitting uncertainty. Solid lines represent the $C(s,0)$ calculated using the model given by Eqs. (7), (8), (9), (10). The solid thick line corresponds to option I, the solid thin line corresponds to option II, the dotted line corresponds to option III. The results of the fits in options (I)–(III) are given in Table 2. The quality of the fit for all options $\chi^2/\mathrm{NDF} \sim 1.3$. The stars correspond to FMO model calculations discussed in Sec. IV

III. EFFECTIVE POMERON APPROACH

The next step was to choose a simple Pomeron contribution to the scattering amplitude, which efficiently describes the data and corresponds to the observed behavior of the curvature $C(s,0)$. In the selected energy region, within the framework of the Regge approach, the contribution of the secondary Reggeons can be neglected, the pp and $\bar{p}p$ scattering differential cross sections are described by the same Pomeron contribution (neglecting

the small correction from Odderon). We chose a common form of the simple Pomeron [11] as

$$A(s,t) = g_i(\tilde{s})^{\alpha_P(t)} e^{\varphi(t)}, \qquad (7)$$

where $\tilde{s} = -i\dfrac{s}{s_0}$, $s_0 = 1$ GeV^2,

$$\alpha_P(t) = 1 + \alpha' t + \gamma(\sqrt{t_0} - \sqrt{t_0 - t}), \qquad (8)$$

$$\varphi(t) = bt + \beta(\sqrt{t_0 - t} - \sqrt{t_0}), \qquad (9)$$

where $\alpha_P(t)$ is a non-linear Pomeron trajectory and $\varphi(t)$ is the non-exponential residue function [9]. The differential cross section has the form

$$\frac{d\sigma}{dt} = \frac{\pi k}{4s^2} |A(s,t)|^2. \qquad (10)$$

Given that originally natural units are used for the model parameters, to get the units of the measured data we apply a conversation factor $k = 0.38938$ mb GeV^2.

Next, we performed an overall (Pomeron) fit of all the above selected 5 sets of data using the model given by Eqs. (7), (8), (9), (10). We consider three options of the combination of the non-exponential behavior by $\varphi(t)$ and the nonlinear trajectory of the Pomeron $\alpha(t)$:

$$\beta \neq \gamma \neq 0 \text{ (I)};$$
$$\beta \neq 0, \gamma = 0 \text{ (II)};$$
$$\beta = 0, \gamma \neq 0 \text{ (III)}.$$

The results of the fits in variants (I)–(III) are given in Table 2. The calculated $C(s,0)$ quantities in options I–III are shown in Fig. 2. Only the behavior of $C(s,0)$ in case (I) has a decreasing character, which completely corresponds to the behavior of the curvature determined directly from the experiment (circles and square). The value of the curvature parameter depending on s changes its sign at asymptotically large energies.

Parameter	I		II		III	
	Value	Error	Value	Error	Value	Error
g_1 for 546 GeV	25.44	0.05	25.34	0.05	25.20	0.04
g_2 for 7 TeV	39.12	0.02	39.19	0.02	39.16	0.02
g_3 for 8 TeV	42.09	0.02	42.07	0.02	42.05	0.02
g_4 for 13 (1) TeV	45.74	0.02	45.77	0.02	45.80	0.02
g_5 for 13 (2) TeV	45.78	0.02	45.81	0.02	45.86	0.02
b, GeV^{-2}	0	fixed	0.5440	0.020	1.128	0.227
α', GeV^{-2}	0.4991	0.0013	0.4684	0.0013	0.4355	0.0023
γ, GeV^{-1}	0.3169	0.0012	0	0	-0.03472	0.00113
β, GeV^{-1}	-1.193	0.024	-0.6245	0.0202	0	0

Table 2. The parameters of the Pomeron fit for (I)–(III) options.

IV. FMO APPROACH

More realistic is the Froissaron and Maximal Odderon approach, which gives a good description of all accessible pp and $\bar{p}p$ elastic scattering at GeV and TeV energies and in a wide $|t|$-range [19, 20]. Let us recall that this is one of the few approximations in which all the basic requirements are taken into account, including both the Froissart theorem for the forward scattering and the Auberson–Kinoshita–Martin theorem for $t \neq 0$. If one includes the latest data from CERN LHC [1, 2] to the analysis, in order to get a proper description, it is necessary to take into account not only the Pomeron, but also the contribution of the Odderon. The simplest form of the scattering amplitude in this case is:

$$P(s,t) = P_0(s,t) + P_1(s,t) + P_2(s,t), \qquad (11)$$

which is the Pomeron contribution.

The simple and dipole Pomerons for both components have a conventional form:

$$P_0(s,t) = -a_{P_0}\tilde{s}^{\alpha_P(t)}e^{\varphi_{P_0}(t)}, \qquad (12)$$

$$P_1(s,t) = -a_{P_1}\tilde{s}^{\alpha_P(t)}e^{\varphi_{P_1}(t)}\ln\tilde{s}, \qquad (13)$$

$$\tilde{s} = -i\frac{s - 2m^2}{2m^2}, $$

$$\alpha_P(t) = 1 + \alpha'_P t, \qquad (14)$$

while the tripole term has the form

$$P_2(s,t) = -\tilde{s}a_{P_2}\frac{2J_1(z_P)}{z_P}e^{\varphi_{P_2}(t)}\ln^2\tilde{s}, \qquad (15)$$

according to the AKM asymptotic theorem,

$$z_P = r_P\tau\ln\tilde{s}, \qquad (16)$$

$$\tau = \sqrt{-t/t_0},\ t_0 = 1\ \text{GeV}^2.$$

The common form of residue functions suggests a nonlinear exponent:

$$\varphi_{P_i}(t) = \beta^{P_i}(\sqrt{t_P} - \sqrt{t_P - t}), \qquad (17)$$

$$t_P = 4m_\pi^2.$$

The contribution of Odderon reads as:

$$O(s,t) = O_0(s,t) + O_1(s,t) + O_2(s,t), \qquad (18)$$

$$O_0(s,t) = ia_{O_0}\tilde{s}^{\alpha_O(t)}e^{\varphi_{O_0}(t)},$$

$$O_1(s,t) = ia_{O_1}\tilde{s}^{\alpha_O(t)}e^{\varphi_{O_1}(t)}\ln\tilde{s},$$

$$O_2(s,t) = i\tilde{s}a_{O_2}\frac{2J_1(z_O)}{z_O}e^{\varphi_{O_2}(t)}\ln^2\tilde{s},$$

$$\varphi_{O_i}(t) = \beta^{O_i}(\sqrt{t_O} - \sqrt{t_O - t}), \qquad (19)$$

$$t_O = 9m_\pi^2, \quad \alpha_O(t) = 1 + \alpha'_O t, \quad z_O = r_O\tau\ln\tilde{s}.$$

In this model we use the following normalization of the total amplitude [11],

$$A_{\bar{p}p}^{pp}(s,t) = P(s,t) \pm O(s,t): \qquad (20)$$

$$\frac{d\sigma}{dt} = \frac{1}{16\pi ks^2}|A_{\bar{p}p}^{pp}(s,t)|^2, \qquad (21)$$

$$\sigma_t(s) = \frac{1}{s}\mathfrak{Im}A_{\bar{p}p}^{pp}(s, t=0), \qquad (22)$$

and

$$\rho(s) = \frac{\mathfrak{Re}A_{\bar{p}p}^{pp}(s, t=0)}{\mathfrak{Im}A_{\bar{p}p}^{pp}(s, t=0)}. \qquad (23)$$

To control the physical meaning of the fitted parameters of differential cross section Eq. (21), we also included the data at $t = 0$ from energy $\sqrt{s} = 546$ GeV up to 13 TeV from compilation [20] to fit with help of Eqs. (22) and (23). The values of the fitted parameters are shown in Table 3.

Pomeron			Odderon		
Parameter	Value	Error	Parameter	Value	Error
a_{P_0}, mb	93.50	5.04	a_{O_0}, mb	−19.06	6.66
a_{P_1}, mb	−9.460	0.692	a_{O_1}, mb	2.823	0.921
a_{P_2}, mb	0.5706	0.0234	a_{O_2}, mb	−0.1157	0.0317
α'_P, GeV^{-2}	0.8868	0.0684	α'_O, GeV^{-2}	0.1766	0.1541
β^{P_0}, GeV^{-1}	2.422	0.213	β^{O_0}, GeV^{-1}	1.099	2.637
β^{P_1}, GeV^{-1}	3.812	fixed	β^{O_1}, GeV^{-1}	2.536	2.451
β^{P_2}, GeV^{-1}	6.211	0.2031	β^{O_2}, GeV^{-1}	3.258	1.655
r_P	0.3514	0.0148	r_O	0.6800	0.0355
Statistics			$\chi^2/\text{NDF} = 0.94$		

Table 3. The values of the fitted parameters of the Froissaron and Maximal Odderon model

In case of this model it is more convenient to consider the slope $B(s)$ and curvature $C(s)$ averaged in some interval of $|t|$ [19]. We did it in the intervals in accordance with Table 4 for TeV energies.

$$\langle B(s)\rangle = \frac{1}{\Delta t}\ln\left(\frac{d\sigma(t_{\min})/dt}{d\sigma(t_{\max})/dt}\right), \qquad (24)$$

where

$$\Delta t = t_{\max} - t_{\min}. \qquad (25)$$

$$\langle C(s)\rangle = \frac{1}{2\Delta t}\left[B(t_{\max}) - B(t_{\min})\right]. \qquad (26)$$

To calculate the slope $B(t)$ at the points $t_{\max}$ and $t_{\min}$, we use the formula for numerical differentiation:

$$B(s,t) = \frac{1}{2\Delta t}\ln\left(\frac{d\sigma(s,t+\Delta t)/dt}{d\sigma(s,t-\Delta t)/dt}\right), \qquad (27)$$

the step was chosen as $\Delta t = 10^{-6}$.

$\sqrt{s}$, GeV^2	$|t_{\min}|$, GeV^2	$|t_{\max}|$, GeV^2	$\langle C(s,t)\rangle$, GeV^{-4}
546	0.0157	0.3500	6.80
7000	0.0132	0.1690	3.64
8000	0.0285	0.1605	3.48
13000	0.0305	0.1300	2.86

Table 4. Averaged curvature and intervals of its calculation

To calculate $\langle C(s)\rangle$ according to the FMO, the interval of momentum transfer with a descending branch of local slope $B(s,t)$ should be selected (see Table 4).

Within these intervals the calculated averaged curvature takes the values given in Table 4.

With the rise in energy, the averaged curvature $\langle C(s)\rangle$ asymptotically decreases (stars in Fig. 2) as in the case of a simple Pomeron with a non-linear trajectory and residue [option (I)].

V. CONCLUSIONS

We have studied the phenomenology of the pp and $\bar{p}p$ elastic scattering within TeV energy range using a model in which the analytical properties of the scattering amplitude are accounted for by the threshold singularity in the t-channel. It has been shown that such features reflect adequately the *"break"* part of the t-dependence of the differential cross-section in the form of a concave curve of the $R(t)$ function. To clarify the question whether the non-exponential behavior of the diffraction cone is due to the nonlinear trajectory or the non-exponential residue function, it is necessary to take into account additionally the novel LHC data. We emphasize that the non-exponential behavior of the function $\varphi(t)$ in the Pomeron pole residue, as well as the non-linearity of the Pomeron trajectory $\alpha(t)$ is strongly suggested by the data. As a result, one can observe that the curvature $C(s,0)$ has a tendency to decrease and change the sign at thousands of TeV (see Fig. 2). It means that the *"asymptopia"* [7] moves to a distant area. Most notably, the same curvature behavior is predicted for the averaged case (see Table 4 and Fig. 2) within the Froissaron and Maximal Odderon (FMO) model that satisfies the basic principles.

ACKNOWLEDGEMENTS

[1] G. Antchev *et al.* (TOTEM Collaboration), Nucl. Phys. B **899**, 527 (2015); https://doi.org/10.1016/j.nucl physb.2015.08.010.

[2] G. Antchev *et al.* (TOTEM Collaboration), Eur. Phys. J. C **79**, 785 (2019); https://doi.org/10.1140/epjc/s 10052-019-7223-4.

[3] G. Antchev *et al.* (TOTEM Collaboration), Eur. Phys. J. C **79**, 881 (2019); https://doi.org/10.1140/epjc/s 10052-019-7346-7.

[4] M. M. Block, L. Durand, P. Ha, F. Halzen, Phys. Rev. D **93**, 114009 (2016); https://doi.org/10.1103/Phys RevD.93.114009/.

[5] J. E. Kontros, A. I. Lengyel, Ukr. Fiz. Zh. **40**, 263 (1995).

[6] P. Desgrolard, J. Kontros, A. I. Lengyel, E. S. Martinov, Nuovo Cim. **110A**, 615 (1997); https://arxiv.org/ab s/hep-ph/9707258.

[7] M. M. Block, B. N. Cahn, Rev. Mod. Phys. **57**, 563 (1985); https://doi.org/10.1103/RevModPhys.5 7.563/.

[8] J. Pumplin, Phys. Lett. B. **276**, 5517 (1992); https://doi.org/10.1016/0370-2693(92)91677-2.

[9] L. Jenkovszky, I. Szanyi, Chung-I Tan, Eur. Phys. J. A **54**, 116 (2018); https://doi.org/10.1140/epja/i2018 -12567-5.

[10] G. Barbiellini *et al.*, Phys. Lett. B **39**, 663 (1972); `https://doi.org/10.1016/0370-2693(72)90025-1/`.

[11] N. Bence, A. I. Lengyel, Z. Z. Tarics, Sci. Herald Uzhhorod Univ. Ser. Phys. **45**, 124 (2019); `https://doi.org/10.24144/2415-8038.2019.45.125-133`.

[12] M. Bozzo *et al.* (UA4 Collaboration), Phys. Lett. **147B**, 385 (1984); `https://doi.org/10.1016/0370-2693(84)90138-2`.

[13] D. Bernard *et al.* (UA4 Collaboration), Phys. Lett. **198B**, 583 (1987); `https://doi.org/10.1016/0370-2693(87)90922-1`.

[14] ATLAS Collabortion, Nucl. Phys. B. **889**, 486 (2014); `https://doi.org/10.1016/j.nuclphysb.2014.10.019/`.

[15] N. A. Amos *et al.* (E-710 Collaboration), Phys. Lett. B **247**, 127 (1990); `https://doi.org/10.1016/0370-2693(90)91060-0`.

[16] V. M. Abazov *et al.* (D0 Collaboration), Phys. Rev. D **86**, 012009 (2012); `https://doi.org/10.1103/PhysRevD.86.012009`.

[17] G. Antchev *et al.* (TOTEM Collaboration), Eur. Phys. J. C **80**, 91 (2020); `https://doi.org/10.1140/epjc/s10052-020-7654-y`.

[18] G. Antchev *et al.* (TOTEM Collaboration), Eur. Phys. Lett. **101**, 21004 (2013); `https://doi.org/10.1209/0295-5075/101/21004`.

[19] E. Martynov, B. Nicolescu, Eur. Phys. J. C **79**, 461 (2019). `https://doi.org/10.1140/epjc/s10052-019-6954-6`.

[20] N. Bence, A. Lengyel, Z. Tarics, E. Martynov, G. Tersomonov, Eur. Phys. J. A **57**, 265 (2021); `https://doi.org/10.1140/epja/s10050-021-00563-z`.

[21] `https://www.hepdata.net`.

ТОНКА СТРУКТУРА ДИФРАКЦІЙНОГО КОНУСА ПРОТОН-ПРОТОННОГО ТА АНТИПРОТОН-ПРОТОННОГО ПРУЖНОГО РОЗСІЮВАННЯ ЗА ЕНЕРҐІЙ ВЕЛИКОГО АДРОННОГО КОЛАЙДЕРА

Н. Бенце[1], І. Сані[2,3,4], О. Лендел[5]

[1] *Ужгородський національний університет, вул. Університетська, 14, Ужгород, Україна,*

[2] *Центр фізичних досліджень ім. Віґнера, п.с. 49, Будапешт, 1525, Угорщина*

[3] *Університеті ім. Етвеша, алея Пазманьї, 1/А, Будапешт, 1117, Угорщина,*

[4] *Технологічний інститут університету МАТЕ, Кампус Роберта Кароля,*
Н-3200, Дендеш, вул. Матраі, 36, Угорщина

[5] *5Інститут електронної фізики НАН України, вул. Університетська, 21, Ужгород, Україна*

Параметр локальної ядерної кривизни як похідну від локального ядерного нахилу відтворено з експериментального диференціального перерізу і пружного розсіювання за енерґій Великого адронного колайдера в ділянці переданого імпульсу, де спостерігаємо "залом". Передбачення кількох моделей померона перевіряємо за при малих переданих імпульсах. Спостерігаємо надзвичайну чутливість параметра локальної ядерної кривизни залежно від вибору моделі померона. Лише деякі з цих моделей проґнозують зменшення параметра локальної ядерної кривизни з енерґією, знак якої змінюється за дуже великих енерґій.

Ключові слова: померон, оддерон, асимптопія, пружне pp і $\bar{p}p$ розсіювання, параметр локальної ядерної кривизни, локальний ядерний нахил.